RSC Advances

PAPER

View Article Online
View Journal | View Issue

Cite this: *RSC Adv.*, 2014, **4**, 11598

Mesoporous composite cathode materials prepared from inverse micelle structures for high performance lithium ion batteries†

Si-Jin Kim,[a] Young-Woo Lee,[a] Bo-Mi Hwang,[a] Seong-Bae Kim,[ab] Woo-Seong Kim,[b] Guozhong Cao[c] and Kyung-Won Park*[a]

Received 8th October 2013
Accepted 6th January 2014

DOI: 10.1039/c3ra45654d

www.rsc.org/advances

Mesoporous $Li_4Mn_5O_{12}/Li_2MnO_3$ composite cathodes are prepared from inverse micelle structures for high-performance LIBs. The relative ratio of layered Li_2MnO_3 to spinel $Li_4Mn_5O_{12}$ in the composite electrodes could be elaborately controlled as a function of molar ratio of $LiNO_3$ to $Mn(NO_3)_2$ (Li/Mn) in the precursor. All $Li_4Mn_5O_{12}/Li_2MnO_3$ composite cathodes exhibit relatively large specific surface areas and mesoporous character, which might be favorable for lithium-ion mobility. The relative ratio of layered Li_2MnO_3 to spinel $Li_4Mn_5O_{12}$ in the composite electrodes were elaborately controlled as a function of molar ratio of $LiNO_3$ to $Mn(NO_3)_2$ (Li/Mn) in the precursor. Our results suggest the better cycle performance of Li excess materials with a solid solution of $Li_4Mn_5O_{12}/Li_2MnO_3$ is due to stabilization of the Li_2MnO_3 structure by addition of a layered component.

1. Introduction

Lithium-ion batteries (LIBs) have been attractive for portable electronic devices due to their excellent electrochemical properties such as high voltage, high energy density and excellent cycling performance. The cathodes in LIBs operate on the principle of reversible intercalation and de-intercalation of lithium ions into/from the transition-metal compound host structure. Among numerous transition metal oxides, lithium cobalt oxide ($LiCoO_2$) is the most common active material.[1] However, since natural deposits of cobalt are scarce, resulting in difficulty in the production of the battery cells at low cost, lithium manganese oxides may be an alternative material to $LiCoO_2$ because of their similar properties to those of $LiCoO_2$. There are several kinds of lithium manganese oxides such as $LiMn_2O_4$,[2,3] $Li_4Mn_5O_{12}$,[4–6] $Li_2Mn_4O_9$,[3,7] $LiMnO_2$ and $Li_{1+\delta}Mn_{2-\delta}O_4$ ($0 < \delta < 0.33$).[8,9] An electromotive force of about 3.0 to 4.0 V can be exhibited when lithium manganese oxides are used as cathode active materials in LIBs.

Manganese oxide-based compounds are particularly attractive as cathodes owing to their lower cost and nontoxicity. However, since various capacity fading problems associated with compounds of Mn with 3.5+ valence state have been identified, numerous efforts have been made to develop substituted manganese oxides with valence state of Mn greater than 3.5+ with better cycling performance. It has been reported that both $Li_4Mn_5O_{12}$[4–6] and Li_2MnO_3[8,10–15] are characterized by a valence state of manganese equal to 4+. Robertson *et al.*[16] reported that Li_2MnO_3 with a monoclinic symmetry (space group of $C2/m$) due to the ordered distribution of Li and Mn in the transition metal layers is electrochemically active with a capacity of 300 mA h g^{-1}. Lim *et al.*[17] synthesized Li_2MnO_3 nanoparticles by a conventional solid-state method, showing a high capacity of 236 mA h g^{-1} by an oxidation reaction process. In $Li_4Mn_5O_{12}$ with spinel structure, the Li atoms are octahedrally coordinated, and the Mn atoms are tetrahedrally coordinated. The spinel type compound exhibits good electrochemical stability at 3 V and is an attractive electrode material for rechargeable 3 V lithium cells.[5] Many reports have, however, emphasized difficulties in preparing $Li_4Mn_5O_{12}$ due to high covalent values of manganese atoms. Johnson *et al.*[8] designed high-performance $0.7Li_2MnO_3 \cdot 0.3Li_4Mn_5O_{12}$ cathodes with high manganese contents synthesized by solid-state reaction and suggested that the layered component is used to achieve high capacity and the spinel component with a three-dimensional interstitial space for Li-ion transport is used to ensure a high-rate capability.

Herein, we prepared mesoporous $Li_2MnO_3/Li_4Mn_5O_{12}$ composite cathodes from inverse micelle structure for high-performance LIBs. The relative ratio of layered Li_2MnO_3 to spinel $Li_4Mn_5O_{12}$ in the composite electrodes were elaborately controlled as a function of molar ratio of $LiNO_3$ to $Mn(NO_3)_2$ (Li/Mn) in the precursor. The structural characterization of

[a]*Department of Chemical Engineering, Soongsil University, Seoul 156-743, Republic of Korea. E-mail: kwpark@ssu.ac.kr*

[b]*Daejung Energy Materials, 740-49 Sinheung-dong, Iksan, Jeonbuk 570-140, Republic of Korea*

[c]*Department of Materials Science and Engineering University of Washington, Seattle, WA 98195, USA*

† Electronic supplementary information (ESI) available. See DOI: 10.1039/c3ra45654d

$Li_2MnO_3/Li_4Mn_5O_{12}$ composite electrodes was carried out using field-emission scanning electron microscopy (FE-SEM), field-emission transmission electron microscopy (FE-TEM) and X-ray diffraction (XRD). The weight ratio of Li to Mn in the electrodes was compared using inductively coupled plasma-atomic emission spectrometry (ICP-AES). The surface area and porosity of the electrodes were analyzed by nitrogen sorption measurement. To evaluate the performance of the electrodes for LIBs, charge–discharge characteristics, cyclic voltammograms (CVs), and cycle performance of cathode materials were measured using lithium coin cells.

2. Experimental

2.1 Materials synthesis

$Li_4Mn_5O_{12}/Li_2MnO_3$ composite cathodes were synthesized using a quaternary medium consisting of water, cyclohexane (Aldrich), lithium dodecyl sulfate (LDS, Aldrich), *n*-butanol (BuOH, Aldrich) and pluronic acid [P123, $(PEO)_{20}$–$(PPO)_{70}$–$(PEO)_{20}$, where PEO is polyethylene glycol and PPO is polypropylene glycol; Aldrich]. The P123 (10.0 g) as a polymer template was dissolved in a mixed solution consisting of 80 g cyclohexane (oil), 9.6 g *n*-butanol (cosurfactant), 0.45 g of LDS (surfactant) and 0.2 g Ketjen black, and was completely stirred until it became optically transparent. To this non-aqueous medium, a 30 mL aqueous solution consisting of 20 mL of 1.5–3.0 M $LiNO_3$ and 10 mL of 1.0 M $Mn(NO_3)_2$ solution in dilute HNO_3 (45–50 wt%) were added. The emulsion was stirred for 20 h followed by slow evaporation at 130 °C to obtain a brown gel. The gel was heated at 300 °C in air for 6 h and a precursor was obtained. Subsequently, the precursor samples were heated at 600 °C in air for 10 h. Then, the powders obtained were collected and washed repeatedly with acetone to remove any possible residual reactant. The sample was then dried in an oven at 60 °C.[18–20]

2.2 Materials characterization

The size and morphology of the electrodes were observed on a FE-SEM (JSM-6700F, Eindhoven) and FE-TEM (Tecnai G2 F30 system operating at 300 kV). For the structure analysis of the catalysts, XRD (D2 PHASER, Bruker AXS) analysis was carried out using a Bruker X-ray diffractometer with a Cu-Kα (λ = 0.15418 nm) source with a Ni filter. The source was operated at 30 kV and 10 mA. The 2θ angular scan from 10 to 80° was explored at a scan rate of 0.5° min^{-1}. Nitrogen adsorption–desorption isotherms were recorded at a model ASAP 2020. The specific surface area was calculated using the Brunauer–Emmett–Teller (BET) method in the relative pressure (P/P_0) range 0.05–0.30 from the adsorption branch of the isotherm. The pore size distribution was calculated by the Barrett–Joyner–Halenda (BJH) method from the desorption branch. Both Li and Mn content of cathode materials were measured, after dissolution, using ICP-AES (Optima-4300 DV, PerkinElmer). Surface chemical composition was examined by X-ray photoelectron spectroscopy (XPS, Thermo VG, U.K.) with a monochromated Al X-ray source (Al-Kα line: 1486.6 eV).

2.3 Electrochemical measurement

To assemble lithium coin cells (size 2032, Hohsen Corporation), the electrodes were fabricated by mixing 80 wt% of cathode samples with 10 wt% Ketjen black as a conducting material (Alfa Aesar) and 10 wt% polyvinylidene difluoride as a binder (Alfa Aesar) in 1-methyl-2-pyrrolidinone solvent (Aldrich, 99%). The mixed slurries were cast onto Al foils as a current collector and dried in air at 100 °C for 12 h. The electrode with an area of 1.32 cm^2 was dried at 70 °C in a vacuum oven. The electrodes were evaluated with respect to lithium foil (FMC Corporation) as a counter electrode. The coin cells were assembled inside an argon-filled glove box (<5 ppm, H_2O and O_2). The positive and negative electrodes of the cells were separated from one another by a porous polypropylene membrane (Wellcos) and an electrolyte solution consisting of 1.4 M $LiPF_6$ in ethylene carbonate : fluoroethylene carbonate : dimethyl carbonate : ethylmethyl carbonate (1 : 1 : 6 : 2) as a solvent mixture (Soulbrain Co., Ltd). Electrochemical impedance spectroscopy measurements (EIS) were performed on the AUTOLAB electrochemical workstation by applying an ac voltage of 5 mV amplitude over the frequency range 100 kHz–0.01 Hz. Before performing impedance spectroscopic measurements the cells were activated through charging to 4.8 V.

3. Results and discussion

3.1 Synthesis and structural analysis of $Li_4Mn_5O_{12}/Li_2MnO_3$ composites

Fig. 1 shows a representation of synthesis of $Li_4Mn_5O_{12}/Li_2MnO_3$ composite cathodes prepared from inverse micelle structures. For the present synthetic approach, the inverse micelle has hydrophilic polar heads inside and hydrophobic nonpolar tail outside (Fig. 1(I)) forming a C_6H_{12} (cyclohexane) atmosphere in contrast to general micelle structures. The

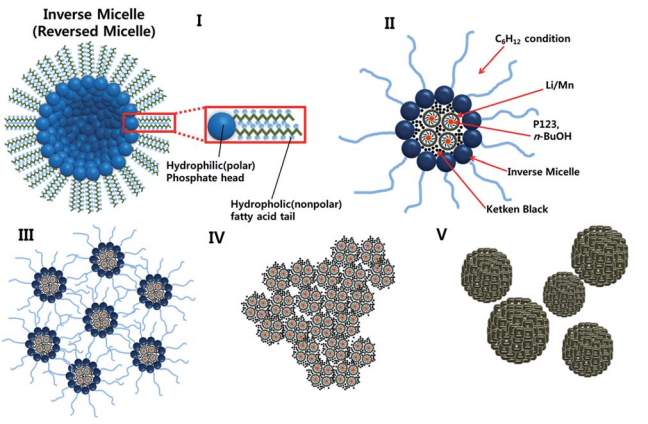

Fig. 1 Schematic illustration of synthesis of the mesoporous $Li_4Mn_5O_{12}/Li_2MnO_3$ composite electrodes prepared using inverse micelle structure. (I) Inverse micelle structure in the present synthesis process. (II) The Li/Mn precursors experimentally added in the inverse micelle structure. (III) The Li/Mn precursor mixture in the composites. (IV) The Li/Mn mixture in the composites after evaporation. (V) The as-prepared mesoporous $Li_4Mn_5O_{12}/Li_2MnO_3$ composites heated at 600 °C.

polymer template, P123 as a block copolymer, consists of polypropylene oxide inside and polyethylene oxide outside and can be expanded by *n*-BuOH with increasing size of the micelle. When the mixture of $LiNO_3$ and $Mn(NO_3)_2$ were added in the cyclohexane atmosphere and infiltrated into the hydrophilic head a spherical shape was generated (Fig. 1(II)). As a result, the Li/Mn mixture was surrounded by the swelling copolymer surfactant forming an emulsion state.

The emulsion was stirred for 20 h followed by slow evaporation at 130 °C to obtain a brown gel (Fig. 1(III)). The gel was heated at 300 °C in air for 6 h, with prevention of agglomeration of the gel by Ketjen black particles (Fig. 1(IV)). Subsequently, the composite materials were obtained by heating at 600 °C for 10 h in air atmosphere (Fig. 1(V)).[21,22]

Fig. 2 shows SEM and TEM images of composite samples prepared as a function of Li/Mn ratio from 1.5 to 3.0 in the precursors. The composite samples prepared with Li/Mn ratio of 1.5 (Fig. 2a), 1.9 (Fig. 2b), 2.5 (Fig. 2c), and 3.0 (Fig. 2d) indicate that all samples seem to be homogeneous spherical particles with a particle size of 600–800 nm (Fig. S1†). As the Li/Mn ratio increases from 1.5 to 3.0, the as-prepared samples turn from dark red–brown to bright red–brown (insets of Fig. 2a–d). The TEM images of Fig. 2e–h indicate that all of the particles consist of small nanoparticles with a size of ~40 nm. As shown in HR-TEM images, the composite samples prepared with Li/Mn ratio from 1.5 to 3.0 display primarily spinel (Li/Mn = 1.5; Fig. S2b†), spinel and layered (Li/Mn = 1.9; Fig. S2d†) and layered (Li/Mn = 2.5 and 3.0; Fig. S2f and h†) structure regions, respectively. The composite sample prepared with Li/Mn ratio of 1.9 mainly show nano-domains structurally integrated by spinel and layered components.[17,23–26]

Fig. 3a shows wide-scan XRD patterns of $Li_4Mn_5O_{12}/Li_2MnO_3$ composite electrodes heated at 600 °C in air atmosphere. In general, cubic spinel $Li_4Mn_5O_{12}$ has a cubic close packed oxygen framework structure and $Fd\bar{3}m$ space group with Mn in the edge-shared octahedral sites. The Li_2MnO_3 has a layered structure with a monoclinic unit cell and $C2/m$ space group. $Li_4Mn_5O_{12}/Li_2MnO_3$ composite electrode prepared with Li/Mn ratio of 1.5 displays a dominant spinel structure of $Li_4Mn_5O_{12}$. However, with increasing Li/Mn from 1.5 to 3.0, the characteristic layered Li_2MnO_3 peaks in the XRD pattern clearly appear at 21.7°. This reveals that the ratio of spinel $Li_4Mn_5O_{12}$ to layered Li_2MnO_3 in the composite electrodes can be controlled through

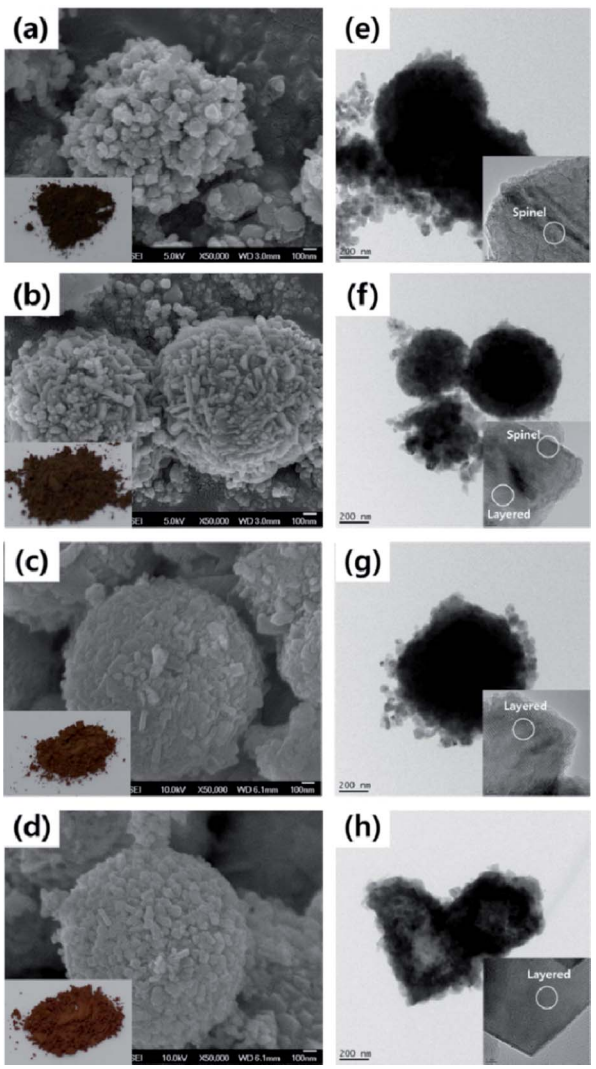

Fig. 2 SEM and TEM images of composite samples prepared with Li/Mn ratio of 1.5 (a and e), 1.9 (b and f), 2.5 (c and g) and 3.0 (d and h).

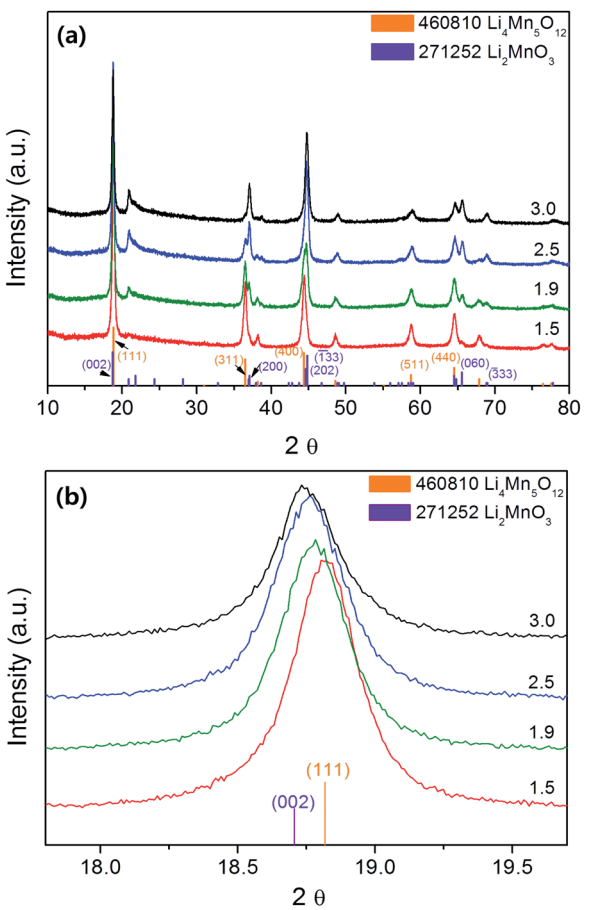

Fig. 3 Wide-scan XRD patterns of $Li_4Mn_5O_{12}/Li_2MnO_3$ composite electrodes heated at 600 °C in air atmosphere.

Table 1 Lattice parameters of $Li_4Mn_5O_{12}/Li_2MnO_3$ composite electrodes prepared with different Li/Mn ratios

	Layered component ($C2/m$)			Spinel component ($F3dm$)
Li/Mn	a/Å	b/Å	c/Å	a/Å
1.5	—	—	—	8.165
1.9	4.928	8.519	9.668	8.179
2.5	4.929	8.474	9.610	8.187
3.0	4.928	8.404	9.600	8.198

Table 2 ICP-AES data of $Li_4Mn_5O_{12}/Li_2MnO_3$ composite electrodes prepared with different Li/Mn ratios

	wt%	
Li/Mn	Li	Mn
1.5	10.214	89.786
1.9	12.033	87.967
2.5	16.582	83.418
3.0	18.653	81.347
$Li_4Mn_5O_{12}$ (JCPDS no. 46-0810)	9.186	90.814
Li_2MnO_3 (JCPDS no. 27-1252)	20.166	79.834

our synthetic approach. As indicated in Fig. 3b, (111) of $Li_4Mn_5O_{12}$ at ~18.817° and (002) of Li_2MnO_3 at ~18.705° are overlapped at around 18.7°. The peaks of $Li_4Mn_5O_{12}/Li_2MnO_3$ composite electrodes prepared with Li/Mn ratio of 1.5, 1.9, 2.5 and 3.0 are located at 18.813, 18.777, 18.754 and 18.724°, respectively, representing a dominant phase transition from spinel $Li_4Mn_5O_{12}$ to layered Li_2MnO_3 with increasing Li/Mn.[8,11,23–25] Typically, a literature value of spinel lattice parameter for $Li_4Mn_5O_{12}$ is a = 8.1616 Å. As shown in Table 1 (obtained using TOPAS, Bruker), the increase in the spinel lattice parameter from a = 8.165 to 8.198 Å for the samples indicates that the spinel component of $Li_4Mn_5O_{12}/Li_2MnO_3$ composite electrodes is reduced with increasing Li/Mn. In contrast, the layered lattice parameters close to the reference values indicate that the layered component of $Li_4Mn_5O_{12}/Li_2MnO_3$ composite electrodes increases with increasing Li/Mn.[8] To clearly characterize the valence state of manganese element in the as-prepared samples, Mn $2p_{3/2}$ spectra of the samples were obtained (Fig. S3†). The spectrum consists of a narrow peak at ~642 eV, a distinct shoulder at ~643 eV, and a broad, pronounced shoulder between 644 and 647 eV. These features are also present in the fitted Mn^{4+} spectrum.[27]

Table 2 shows ICP-AES data of weight percentage (wt%) of Li and Mn in $Li_4Mn_5O_{12}/Li_2MnO_3$ composite electrodes with respect to $Li_4Mn_5O_{12}$ and Li_2MnO_3 as references. For reference, the weight ratio of (Li : Mn) for single $Li_4Mn_5O_{12}$ and Li_2MnO_3 are (9.186 : 90.814) and (20.166 : 79.834), respectively. The weight ratios of (Li : Mn) in $Li_4Mn_5O_{12}/Li_2MnO_3$ composite electrodes prepared with Li/Mn ratio of 1.5, 1.9, 2.5 and 3.0 are 10.214 : 89.786, 12.033 : 87.967, 16.582 : 83.418, 18.653 : 81.347, respectively, indicating phase transition from $Li_4Mn_5O_{12}$ to Li_2MnO_3 with increasing Li/Mn. Based on the

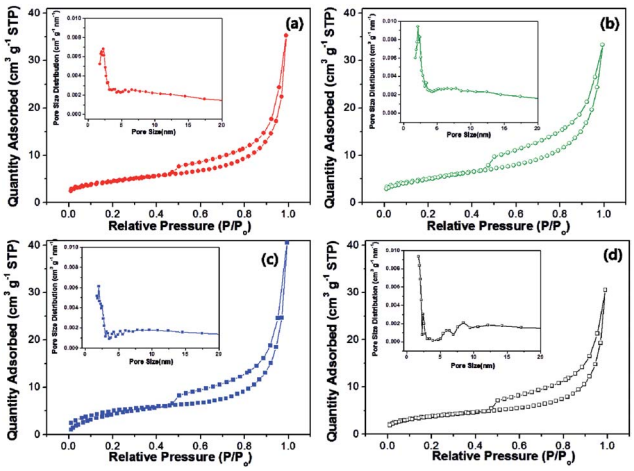

Fig. 4 Nitrogen adsorption–desorption isotherms of $Li_4Mn_5O_{12}/Li_2MnO_3$ composite electrodes prepared with Li/Mn ratios of (a) 1.5, (b) 1.9, (c) 2.5 and (d) 3.0. and inset pore size distribution (BJH) curves of $Li_4Mn_5O_{12}/Li_2MnO_3$ composite samples.

peak position from XRD patterns (Fig. 2b) and the Li/Mn ratio from ICP-AES data (Table 2), it is observed that the relative ratio of $Li_4Mn_5O_{12}$ to Li_2MnO_3 in the composite samples can be varied as a function of the Li/Mn ratio in the present synthetic process.

Furthermore, in order to characterize the pore structure of the samples, nitrogen gas adsorption–desorption isotherms and pore size distribution curves of the $Li_4Mn_5O_{12}/Li_2MnO_3$ composite electrodes were obtained as shown in Fig. 4. The isotherm curves of the composite samples display a well-defined step for the relative pressure P/P_o ranging from 0.6 to 0.8 as a typical IV classification with a clear H1-type hysteretic loop, which is characteristic of mesoporous materials. $Li_4Mn_5O_{12}/Li_2MnO_3$ composite electrodes prepared with Li/Mn ratios of 1.5, 1.9, 2.5 and 3.0 have specific surface areas of 16.2, 20.4, 18.9 and 16.8 $m^2\ g^{-1}$ and mesoporous character, which might be favorable for lithium-ion mobility.[29] The pore size distribution curve of the all samples is mesoporous with pore diameter of ~2.5 nm with narrow size distribution corresponding to the replication of the samples (Fig. 2).[29]

3.2 Electrochemical analysis of the $Li_4Mn_5O_{12}/Li_2MnO_3$ composite cathodes

Fig. 5a–d shows 1st and 2nd charge–discharge curves of $Li_4Mn_5O_{12}/Li_2MnO_3$ composite cathodes at a current density of 0.1 C. At 0.1 C, the 1st discharge capacities of $Li_4Mn_5O_{12}/Li_2MnO_3$ composite cathodes prepared with Li/Mn ratios of 1.5, 1.9, 2.5 and 3.0 are 199.84, 269.41, 184.78 and 182.01 m Ah g^{-1}, respectively. However, total capacities of $Li_4Mn_5O_{12}/Li_2MnO_3$ composite cathodes contain complicated electrochemical contributions from layered and spinel components. Recently, Johnson *et al.* demonstrated the stages in the discharge curves of $Li_4Mn_5O_{12}/Li_2MnO_3$ composite cathodes assigned to the spinel, layered or both dominant regions.[8,11] In our case, the profile of the discharge curves of a lithium cell with the

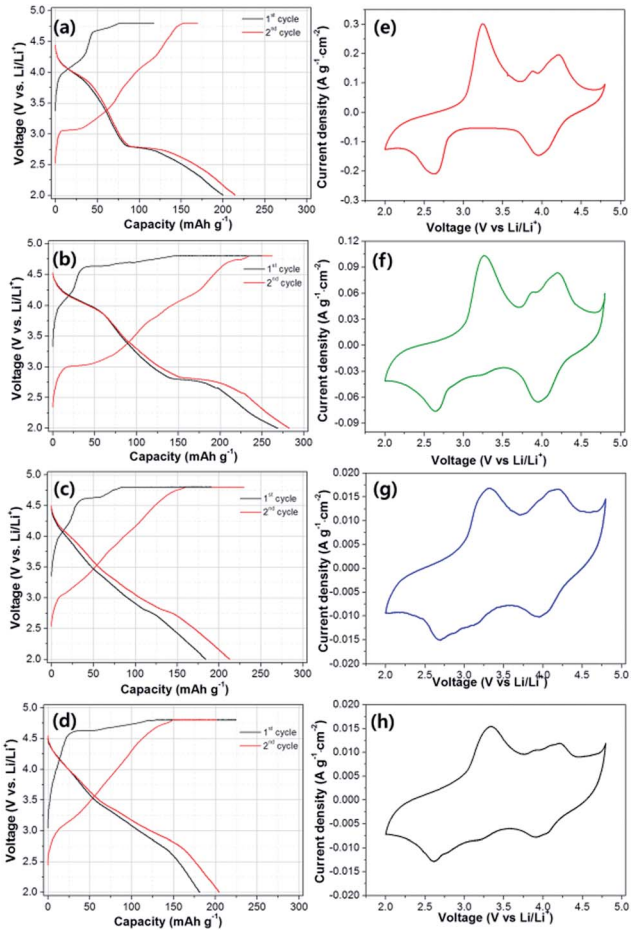

Fig. 5 Charge–discharge curves and CVs of $Li_4Mn_5O_{12}/Li_2MnO_3$ composite cathodes prepared with Li/Mn ratio of 1.5 (a and e), 1.9 (b and f), 2.5 (c and g) and 3.0 (d and g).

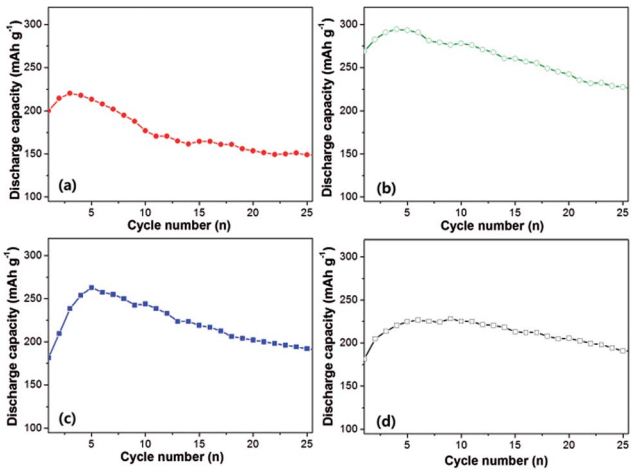

Fig. 6 Plots of specific discharge capacity *vs.* cycle number for $Li_4Mn_5O_{12}/Li_2MnO_3$ composite cathodes prepared with Li/Mn ratios of (a) 1.5, (b) 1.9, (c) 2.5 and (d) 3.0 at room temperature.

cathodes can be classified by four distinct regions: initial (4.8–3.8 V), layered (3.8–2.8 V), spinel (2.8–2.7 V), and layered/spinel (2.7–2.0 V), resulting from the composite character with spinel $Li_4Mn_5O_{12}$ and layered Li_2MnO_3. Table 3 displays comparison of discharge capacities divided by the four stages of $Li_4Mn_5O_{12}/Li_2MnO_3$ composite cathodes. In particular, in the layered region between 3.8 and 2.8 V, the capacities of the composites prepared with Li/Mn ratios of 1.5, 1.9, 2.5 and 3.0 are 21.41, 28.26, 44.15 and 52.55%, respectively. In contrast, in the spinel region between 2.8 and 2.7 V, the capacities of the composites prepared with Li/Mn ratios of 1.5, 1.9, 2.5 and 3.0 are 16.41, 15.21, 8.66 and 4.17%, respectively. This indicates that the portion of the layered component increases with increasing Li/Mn whereas the contribution of the spinel component decreases, which is in good agreement with both XRD and ICP-AES analysis (Fig. 3).[28,29] Fig. 5e–h show CVs of lithium coin cells using $Li_4Mn_5O_{12}/Li_2MnO_3$ composite cathodes with a scan rate of 0.2 mV s^{-1} in the range between 4.8 and 2.0 V *vs.* Li/Li^+. The representative reduction peaks appear at ~4.0 and ~2.7 V. In particular, the layered component in the composite cathodes has the reduction region between 3.8 and 2.8 V. With increasing Li/Mn from 1.5 to 3.0, a reduction peak corresponding to the discharge in the layered structure for the composite cathodes can be clearly observed in the potential range.[30–36]

The cycling performance of the composite cathodes for 25 cycles at a current rate of 0.1 C is indicated in Fig. 6. The early stage between the 1st and 5th cycles of composite cathodes during the cycling reaction exhibits an activation process.[17,20] The composite cathodes prepared with Li/Mn ratio of 1.5, 1.9 and 2.5 exhibit 199.84, 269.27, and 184.78 mA h g^{-1} of 1st discharge capacity and 71.02, 77.04 and 72.51% of capacity retention after maximum capacitance to 25 cycles, respectively.. The 1st and 25th discharge capacities of the composite cathode prepared with Li/Mn ratio of 3.0 are 180.01 and 190.12 mA h g^{-1}, respectively, *i.e.* greater than its initial capacity after 25 cycles. The unusually retained capacity is shown in Fig. 6d.

Nyquist plots of the $Li_4Mn_5O_{12}/Li_2MnO_3$ composite electrodes were obtained as shown in Fig. 7a. The impedance

Table 3 Comparison of discharge capacities for $Li_4Mn_5O_{12}/Li_2MnO_3$ composite cathode materials prepared with different Li/Mn ratios

	Capacity (mA h g^{-1})/portion (%)							
Potential range	Li/Mn = 1.5		Li/Mn = 1.9		Li/Mn = 2.5		Li/Mn = 3.0	
Initial (4.8–3.8 V)	39.24	19.63	64.18	23.81	28.98	15.67	36.08	19.82
Layered (3.8–2.8 V)	42.78	21.41	76.15	28.26	81.57	44.15	95.64	52.55
Spinel (2.8–2.7 V)	32.79	16.41	41.01	15.21	15.99	8.66	7.59	4.17
Layered + spinel (2.7–2.0 V)	85.03	42.55	88.07	32.72	58.24	31.52	42.7	23.46
Total	199.84	100	269.41	100	184.78	100	182.01	100

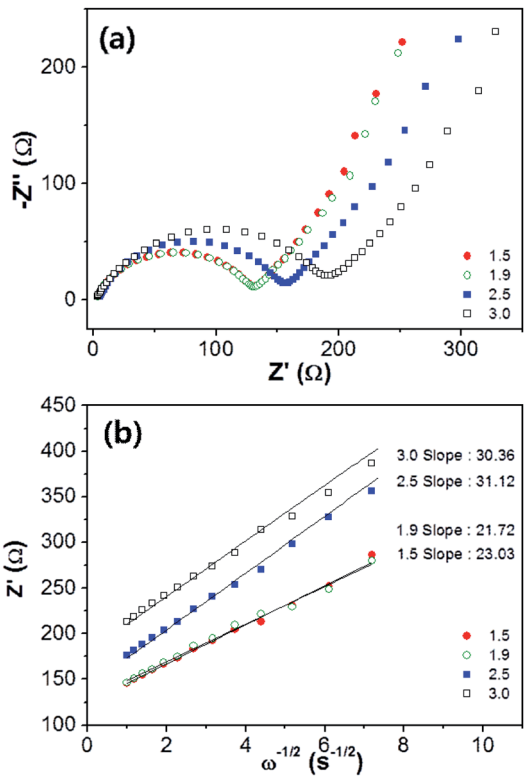

Fig. 7 (a) Nyquist plots of $Li_4Mn_5O_{12}/Li_2MnO_3$ composite samples in the frequency range between 100 kHz and 0.01 Hz. (b) The relationship between Z_{Re} and $\omega^{-1/2}$ at low frequency.

Table 4 Comparison of charge transfer resistance (R_{ct}), Warburg impedance coefficient (σ_W), and diffusion coefficient (D) of the composite electrodes

Li/Mn	R_{ct}/Ω	$W/\Omega\ cm^2\ s^{-1/2}$	$D/cm^2\ s^{-1}$
1.5	130	23.03	4.05×10^{-14}
1.9	128	21.72	4.56×10^{-14}
2.5	157	31.12	2.27×10^{-14}
3.0	198	30.36	2.33×10^{-14}

spectra of the cell consisted of two depressed semicircles in the high-to-medium frequency region and a straight line in the low frequency region. The value of the diameter of the semicircle on the Z real axis is related to the charge transfer resistance (R_{ct}). The values of R_{ct} of the $Li_4Mn_5O_{12}/Li_2MnO_3$ composite electrodes prepared with Li/Mn ratios of 1.5, 1.9, 2.5 and 3.0 are 130, 128, 157 and 198 Ω. The low frequency region of the straight line is attributed to the Warburg diffusion of the lithium ions into the electrode material (Table 4).

$$Z_{Re} = R_e + R_{ct} + \sigma_W \omega^{-1/2} \quad (1)$$

$$D = R^2T^2/2A^2n^4F^4C^2\sigma_W{}^2 \quad (2)$$

From eqn (2), the Li-ion diffusion coefficients (D) of the $Li_4Mn_5O_{12}/Li_2MnO_3$ composite electrodes prepared with Li/Mn ratios of 1.5, 1.9, 2.5 and 3.0 can be obtained as 4.05×10^{-14}, 4.56×10^{-14}, 2.27×10^{-14} and 2.33×10^{-14} $cm^2\ s^{-1}$, respectively, exhibiting much faster Li-ion diffusion process in the composite electrode prepared with Li/Mn ratio of 1.9. As a result, the improved lithium-ion intercalation properties of the composite electrode prepared with Li/Mn ratio of 1.9 is believed to be attributed to relatively large specific surface area, low transport resistance, and high lithium ion diffusion coefficient in the mesoporous nanostructured electrode.[37]

4. Conclusion

We have successfully prepared mesoporous $Li_2MnO_3/Li_4Mn_5O_{12}$ composite cathodes for high-performance LIBs by means of a modified inverse micelle method. The ratio of layered Li_2MnO_3 to spinel $Li_4Mn_5O_{12}$ in the composite electrodes could be controlled as a function of Li/Mn. All $Li_4Mn_5O_{12}/Li_2MnO_3$ composite cathodes exhibit relatively large specific surface areas and mesoporous character, which might be favorable for lithium-ion mobility. The total discharge capacities of $Li_4Mn_5O_{12}/Li_2MnO_3$ composite cathodes are a sum of the electrochemical contributions by layered and spinel components.

Acknowledgements

This work was supported by the IT R&D program of MKE/KEIT [KI002176, Development of 3.6 A h Class Cylindrical Type Lithium Secondary Battery] and the Human Resources Development program (no. 20124030200070) of the Korea Institute of Energy Technology Evaluation and Planning (KETEP) grant funded by the Korea government Ministry of Trade, Industry and Energy.

References

1 B. L. Ellis, K. T. Lee and L. F. Nazar, *Chem. Mater.*, 2010, **22**, 691.
2 F. Lubin, A. Lecerf, M. Broussely and J. Labat, *J. Power Sources*, 1991, **34**, 161.
3 M. M. Thackeray, A. de Kock, M. H. Rossouw, D. Liles, R. Bittihn and D. Hoge, *J. Electrochem. Soc.*, 1992, **139**, 363.
4 Y. Tanaka, Q. Zhang and F. Saito, *Powder Technol.*, 2003, **132**, 74.
5 Y. Tian, D. Chen, X. Jiao and Y. Duan, *Chem. Commun.*, 2007, 2072.
6 Y. Zhao, Q. Lai, Y. Hao, H. Zeng, H. Chu and Z. Lin, *J. Power Sources*, 2010, **195**, 4400.
7 C. Masquelier, M. Tabuchi, K. Ado, R. Kanno, Y. Kobayashi, Y. Maki, O. Nakamuraand and J. B. Goodenough, *J. Solid State Chem.*, 1996, **123**, 255.
8 C. S. Johnson, N. Li, J. T. Vaughey, S. A. Hackney and M. M. Thackeray, *Electrochem. Commun.*, 2005, **7**, 528.
9 P. Strobel, F. L. Cras and M. Anne, *J. Solid State Chem.*, 1996, **124**, 83.
10 G. Jain, J. Yang, M. Balasubramanian and J. J. Xu, *Chem. Mater.*, 2005, **17**, 3850.

11 M. M. Thackeray, S.-H. Kang, C. S. Johnson, J. T. Vaughey, R. Benedek and S. A. Hackney, *J. Mater. Chem.*, 2007, **17**, 3112.
12 C. S. Johnson, N. Li, C. Lefief, J. T. Vaughey and M. M. Thackeray, *Chem. Mater.*, 2008, **20**, 6095.
13 C. Yu, G. Li, X. Guan, J. Zheng, D. Luo and L. Li, *Phys. Chem. Chem. Phys.*, 2012, **14**, 12368.
14 M. M. Thackeray, S.-H. Kang, C. S. Johnson, J. T. Vaughey and S. A. Hackney, *Electrochem. Commun.*, 2006, **8**, 1531.
15 M. M. Thackeray, C. S. Johnson, J. T. Vaughey, N. Li and S. A. Hackney, *J. Mater. Chem.*, 2005, **15**, 2257.
16 A. D. Robertson and P. G. Bruce, *Chem. Commun.*, 2002, 2790.
17 J. S. Lim, J. E. Moon, J. H. Gim, S. J. Kim, K. K. Kim, J. J. Song, J. W. Kang, W. B. Im and J. K. Kim, *J. Mater. Chem.*, 2012, **22**, 11772.
18 N. N. Sinha and N. Munichandraiah, *J. Electrochem. Soc.*, 2010, **157**, A647.
19 F. Kleitz, J. Blanchard, B. Zibrowius and F. Schüth, *Langmuir*, 2002, **18**, 4963.
20 A. Jusufi, A.-P. Hynninen and A. Z. Panagiotopoulos, *J. Phys. Chem. B*, 2008, **112**, 13783.
21 P. Feng, X. Bu and D. J. Pine, *Langmuir*, 2000, **16**, 5304.
22 K. S. Liu, H. G. Fu, K. Shi, F. S. Xiao, L. Q. Jing and B. F. Xin, *J. Phys. Chem. B*, 2005, **109**, 18719.
23 A. D. Robertson and P. G. Bruce, *Chem. Mater.*, 2003, **15**, 1984.
24 A. Boulineau, L. Croguennec, C. Delmas and F. Weill, *Chem. Mater.*, 2009, **21**, 4216.
25 X. Zhang, C. Yu, X. D. Huang, J. Zheng, X. F. Guan, D. Luo and L. P. Li, *Electrochim. Acta*, 2012, **81**, 233.
26 H. Yu and H. S. Zhou, *J. Phys. Chem. Lett.*, 2013, **4**, 1268.
27 H. W. Nesbitt and D. Banerjee, *Am. Mineral.*, 1998, **83**, 305.
28 Y.-K. Sun, M.-J. Lee, C. S. Yoon, J. Hassoun, K. Amine and B. Scrosati, *Adv. Mater.*, 2012, **24**, 1192.
29 S. B. Schougaard, J. Bréger, M. Jiang, C. P. Grey and J. B. Goodenough, *Adv. Mater.*, 2006, **18**, 905.
30 J. Y. Baek, H.-W. Ha, I.-Y. Kim and S.-J. Hwang, *J. Phys. Chem. C*, 2009, **113**, 17392.
31 C. S. Johnson, J.-S. Kim, C. Lefief, N. Li, J. T. Vaughey and M. M. Thackeray, *Electrochem. Commun.*, 2004, **6**, 1085.
32 N. Yabuuchi, K. Yoshii, S.-T. Myung, I. Nakai and S. Komaba, *J. Am. Chem. Soc.*, 2011, **133**, 4404.
33 J. R. Croy, K. G. Gallagher, M. Balasubramanian, Z. Chen, Y. Ren, D. Kim, S.-H. Kang, D. W. Dees and M. M. Thackeray, *J. Phys. Chem. C*, 2013, **117**, 6525.
34 S.-H. Yu, T. Yoon, J. Mun, S. Park, Y.-S. Kang, J.-H. Park, S. M. Oh and Y.-E. Sung, *J. Mater. Chem. A*, 2013, **1**, 2833.
35 R. Marom, S. F. Amalraj, N. Leifer, D. Jacob and D. Aurbach, *J. Mater. Chem.*, 2011, **21**, 9938.
36 H. I. Wu, G. Chan, J. W.Choi, I. Ryu, Y. Yao, M. T. Mcdowell, S. W. Lee, A. Jackson, Y. Yang, L. B. Hu and Y. W. Cui, *Nat. Nanotechnol.*, 2012, **7**, 310.
37 Y. M. Lin, K. C. Klavetter, P. R. Abel, N. C. Davy, J. L. Snider, A. Heller and C. Mullins, *Chem. Commun.*, 2012, **48**, 7268.